Nano Energy 65 (2019) 103902

Contents lists available at ScienceDirect

Nano Energy

journal homepage: www.elsevier.com/locate/nanoen

Full paper

Salt-controlled dissolution in pigment cathode for high-capacity and long-life magnesium organic batteries

Lianmeng Cui[a], Limin Zhou[a], Kai Zhang[b], Fangyu Xiong[a], Shuangshuang Tan[a], Maosheng Li[a], Qinyou An[a,**], Yong-Mook Kang[b], Liqiang Mai[a,*]

[a] State Key Laboratory of Advanced Technology for Materials Synthesis and Processing, International School of Materials Science and Engineering, Wuhan University of Technology, Wuhan, 430070, Hubei, PR China
[b] Department of Energy and Materials Engineering, Dongguk University-Seoul, Seoul, 04620, Republic of Korea

ARTICLE INFO

Keywords:
Organic electrode
Magnesium batteries
PTCDA
Voltage platform
Dissolution inhibition

ABSTRACT

Benefiting from high volumetric energy density and generally dendrite-free growth of Mg metal, rechargeable magnesium batteries (MBs) become a promising next-generation energy storage system. Organic electrode materials, with characteristic of sustainable resource and flexible structure, have been widely studied in alkali metal ion batteries, but are rarely reported in MBs. Herein, we demonstrate that 3,4,9,10-perylenetetracarboxylic dianhydride (PTCDA) serves as a cathode material for MBs in non-aqueous system, which realizes a fast diffusion kinetics and remarkable Mg-storage performance through a salt-dissolution inhibition approach for the electrolyte. The PTCDA exhibits a reversible capacity of 126 mAh g^{-1} (at 200 mA g^{-1}), excellent rate performance, and good cycling stability (100 mAh g^{-1} even after 150 cycles). Furthermore, the evolution mechanism of the PTCDA electrode based on the transformation between carbonyl groups (C═O) and enolate groups (C–O) is revealed by *ex-situ* phase characterization and functional group analysis. Besides, the dissolution inhibition of the PTCDA could also be realized through the incorporation of other soluble salt (KCl or NaCl) into all phenyl complex (APC) electrolyte, resulting in an enhanced cycling capacity. Considering the designable configuration of the organic materials, this work would pave way for their utilization on multi-valent ion batteries and provide efficient strategy to realize high voltage and satisfied cycle life.

1. Introduction

Confronted with the wide utilization and the large-scale demand of energy storage system, the development of lithium-ion batteries (LIBs) has reached a bottleneck due to the low reserves of lithium, limited energy density, and safety issues of LIBs during the repeated cycling. Therefore, developing the next-generation battery system is very essential to meet increasing requirements. Benefiting from high volumetric energy density (3833 mAh cm^{-3}) and dendritic-free growth during the repeated cycling, rechargeable magnesium batteries (MBs) are considered to be one of the promising candidates as supplement or substitute for energy storage devices. Besides, Mg metal anode material, features cheap price and abundant light metal reserves element (1.5 wt % in earth crust) [1,2]. In 2000, based on Mg metal anode and Chevrel phase Mo_6S_8 cathode combined with $Mg(AlCl_2EtBu)_2$/Tetrahydrofuran (THF) as the electrolyte, D. Aurbach et al. developed a magnesium secondary battery prototype, which achieved a 100% Coulombic efficiency of the magnesium deposition-dissolution cycles and a charge capacity of ~122 mAh g^{-1} [3]. However, there is a low operation voltage and specific capacity for Mo_6S_8 as a Mg-storage material, resulting in a limited energy density of MBs. The major challenge for MBs resides in the strong intercalation between divalent Mg^{2+} ions and the host materials, causing a low ion diffusion kinetic, poor discharge capacity, and undesirable cycling stability. Various Mg-storage cathode materials have been successively proposed, such as transition-metal sulfides (VS_4 [4], TiS_2 [5,6], MoS_2 [7,8], CuS [9]), transition-metal oxides (V_2O_5 [10,11], fluorine doping $\alpha-MoO_3$ [12]), and polyanionic compounds ($Mg_{1.03}Mn_{0.97}SiO_4$ [13,14], $MgMnSiO_4$ [15], $MgFeSiO_4$ [16]). Unfortunately, most of these materials are difficult to synthesize and their Mg-storage performance could not rival with the Chevrel phase Mo_6S_8. As a result, exploring suitable cathode materials with high operation voltage and specific capacity is of great significance.

The organic materials, typical of structural designability and chemical diversity, have been widely studied in LIBs [17–19] and sodium-

* Corresponding author.
** Corresponding author.
E-mail addresses: anqinyou86@whut.edu.cn (Q. An), mlq518@whut.edu.cn (L. Mai).

https://doi.org/10.1016/j.nanoen.2019.103902
Received 28 March 2019; Received in revised form 10 July 2019; Accepted 12 July 2019
Available online 27 July 2019

ion batteries (SIBs) [20,21]. However, there are few reports about their application on rechargeable magnesium batteries [22–25]. Recently, Liao et al. demonstrated 2,5-dimethoxy-1,4-benzoquinone (DMBQ) as cathode material for rechargeable MBs, delivering an initial capacity of 226 mAh g^{-1} (at 0.2 C) and retaining 74 mAh g^{-1} after 30 cycles [26]. They discovered that the electrode material has a considerable capacity loss upon cycling, and there is much room for further optimization of the organic Mg-storage electrodes. 3,4,9,10-perylenetetracarboxylic dianhydride (PTCDA), known as organic pigment "red 224", is composed of one aromatic ring center and two anhydride groups, and further stacks forming the PTCDA crystals through the π-π stacking between layers. Ji et al. assembled a three-electrode magnesium cell with an aqueous electrolyte (4.8 M $Mg(NO_3)_2$), in which PTCDA served as working electrode, activated carbon as counter electrode, and Ag/AgCl (in sat. KCl) as reference electrode. It displayed a reversible capacity of ~125 mAh g^{-1} at 20 mA g^{-1} [27]. Considering the initial research purpose of MBs, the advantage of the magnesium anode was not utilized at all, which actually limited the application of PTCDA. In view of passivation of Mg metal in an aqueous electrolyte, the PTCDA as Mg-storage material in non-aqueous system is worthy to be attempted [28,29]. According to the reaction mechanism of the PTCDA in alkali metal ion batteries, each PTCDA molecule can transfer two electrons during the charge/discharge process in the voltage range from 0.6 V to 2.5 V (Scheme 1), and the corresponding theoretical capacity of PTCDA is about 144 mAh g^{-1}. Thus, it is important to realize high magnesium storage activity of the PTCDA in organic electrolyte system for its further development and practical application.

Herein, we assembled the coin cells using Mg foil as anode, PTCDA as cathode, and aluminum chloride THF complex/phenylmagnesium chloride (all phenyl complex, APC) solution as non-aqueous electrolyte. Considering the dissolution issue of organic materials in aprotic electrolyte, the incorporate of the dissolvable salt (1 M LiCl) in electrolyte was adopted to maximize the utilization of the active material. And the PTCDA displays an excellent electrochemical performance. Besides, the behavior of dissolution inhibition is directly observed and measured via Fourier transform infrared spectroscopy (FTIR) and ultraviolet visible (UV–vis) absorption spectrum. The electrochemical enolization mechanism of the PTCDA is also verified through the track of phase change and functional group. Significantly, KCl and NaCl salts also play an identical role on reducing the solubility of PTCDA to achieve a good cycling performance. This study offers a general approach to maximize the utilization of electrode materials and enhance their Mg-storage performance, especially for sustainable organic materials.

2. Results and discussion

Fig. 1a shows the X-ray diffraction (XRD) pattern of the commercial PTCDA powder. It displays a β-crystalline and the monoclinic $P2_1/c$ space group, and the diffraction peaks located at 9.3, 12.1, 24.3, and 27° can be ascribed to (011), (021), (042) and (102) planes, respectively [30]. The scanning electron microscopy (SEM) image (inset of Fig. 1a) shows that PTCDA has a micro-rod morphology with the length of 500 nm and width of 200 nm. Considering high solubility of the

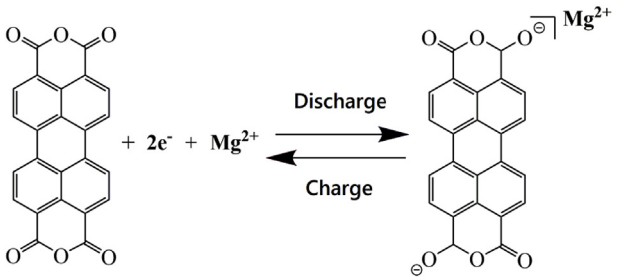

Scheme 1. Theoretical reaction mechanism of the PTCDA electrode as cathode.

organic electrode material in alkali metal ion batteries, the dissolution problem is first measured to evaluate the availability of the PTCDA material in MBs. From the comparison of dissolution experiments in electrolyte with different soak time, the color is nearly unchanged for the APC electrolyte containing LiCl with the increasing of soak time from 1 to 24 h, which indicating a possible dissolution inhibition property for PTCDA in this sample (Fig. 1b). Fig. S1 presents the morphology of the PTCDA electrode before and after soaking 24 h in the two electrolytes. The morphology of the PTCDA has no significant change after soaking in APC electrolyte with LiCl, while the other one partially dissolved in APC electrolyte. Noted that all the electrodes soaked in electrolyte were washed for several times (3~5) to remove the redundant electrolyte. The FTIR spectrogram of the PTCDA powder is shown in Fig. S2, and the absorbance peak at 1767 cm^{-1} can be attributed to the vibrational modes of the C=O double bonds in PTCDA. The peaks centered at 1591, 1505, and 1405 cm^{-1} belong to the C=C double bonds, and 863, 805, and 733 cm^{-1} can be attributed to the C–H bond [30]. Besides, the FTIR spectra (Fig. 1c) demonstrate that the transmittance of electrolyte containing LiCl does not obviously change, illustrating that the PTCDA has low solubility in this electrolyte. With respect to the electrolyte without LiCl, the peaks located at ~1750 cm^{-1} and 700 cm^{-1} obviously change, which are ascribed to the dissolution of the PTCDA. Fig. 1d shows the UV–vis spectra of the electrolytes collected after soaking 24 h. The absorption peaks at 470 and 510 nm are ascribed to the dissolved PTCDA and the peaks of APC electrolyte are stronger than in electrolyte with LiCl, illustrating that the PTCDA has lower solubility in the electrolyte with LiCl. Through the visual observation, the color change of the separator (Fig. S3) assembled in APC electrolyte is deeper than the one with LiCl. Integrated analysis of these results is that the dissolution of PTCDA can be effectively suppressed with the addition of LiCl.

To investigate the electrochemical properties of the PTCDA, the coin-type batteries were assembled using Mg foil as anode, PTCDA as cathode, and glass fiber (GF/A) as the separator. Here, molybdenum foil was placed to avoid the side reaction between the electrolyte and the stainless steel shell. To value the available voltage range of the electrolyte, the cyclic voltammetry (CV) curves of the APC electrolyte with/without LiCl are shown in Fig. S4. We can see that the high cut-off voltage is limited to 2.5 V (*vs.* Mg/Mg^{2+}) because of the compatibility of Mg foil combine with APC electrolyte in magnesium battery system. As Fig. S5 shows, the PTCDA electrode possesses an initial capacity of 130 mAh g^{-1} (at 100 mA g^{-1}) when cycling between the voltage range from 0.6 to 2.5 V in APC electrolyte. All the capacities in this work are calculated based on the mass of the PTCDA. After 50 cycles, the reversible capacity is only 75 mAh g^{-1}. The rapid capacity decay is possibly attributed to the dissolution of the host material in APC electrolyte. Then different concentrations of LiCl (0.2, 0.5, 0.8, 1.0, and 1.5 M) are added into the APC electrolyte. And LiCl cannot completely dissolve when the concentration is 1.5 M. Comparing the electrochemical performance with different electrolytes, the decay of the reversible capacity is much slower than that in APC electrolyte when the LiCl is beyond 0.5 M. In order to exclude the factor of the APC electrolyte concentration, we assemble coin cells used 0.4 M APC electrolyte to demonstrate the cycling stability of the PTCDA. The battery system delivers a capacity of 67 mAh g^{-1} after 70 cycles (Fig. S6). Based on the above experiments, the dissolution of the PTCDA is inhibited by adding LiCl salt, which is consistent with the results of UV–vis and FTIR spectrograms. The capacity of the cathode material is improved with the concentration of LiCl increasing from 0 M to 0.8 M. With the concentration of LiCl above 1.0 M, however, the capacity reduces due to the diffusion kinetic of Mg^{2+} inhibited by the high viscosity of electrolyte [31]. The charge/discharge plateaus have no obvious change with the different concentration of LiCl (Fig. S7). The salt concentration is a trade-off among solubility, ionic conductivity, and viscosity. Considering these factors, the PTCDA displays the best cycling stability when cycled in the 1.0 M LiCl-APC electrolyte (Fig. 2a). Fig. 2b

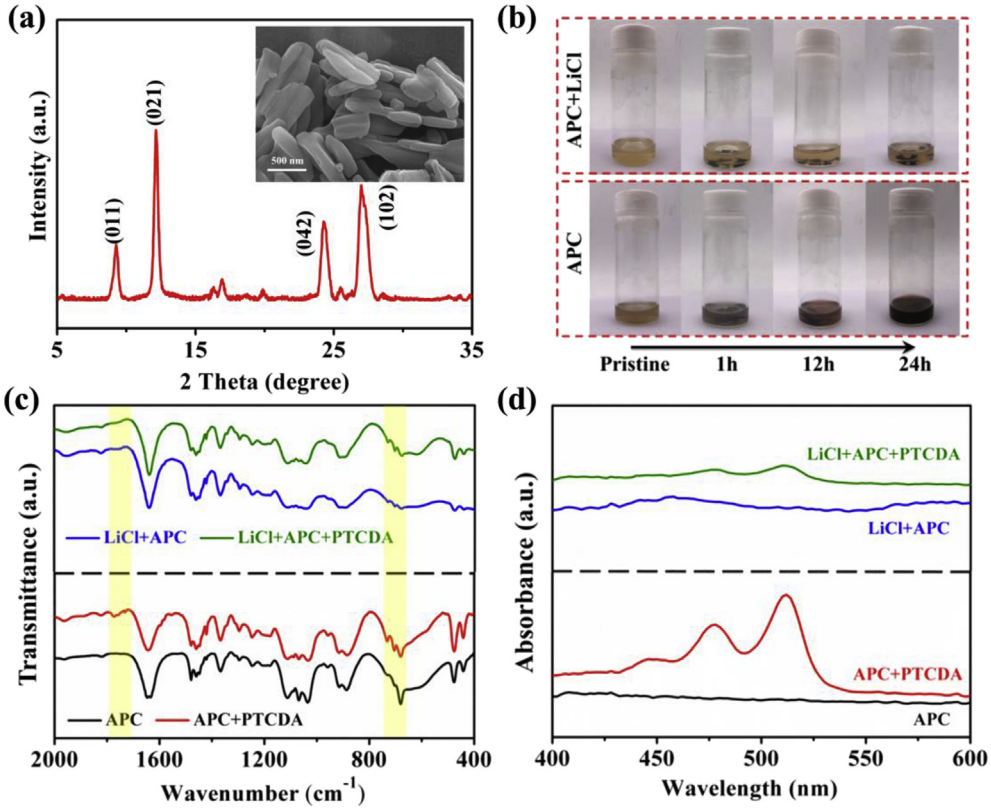

Fig. 1. The dissolution of PTCDA in APC electrolyte with/without LiCl. (a) The XRD pattern of the PTCDA (inset: SEM image of the PTCDA); (b) digital photos of the PTCDA dissolved in different electrolytes with different soak time; (c) FTIR and (d) UV–vis spectra of the PTCDA in the APC electrolyte with/without LiCl.

shows the rate performance of the PTCDA. The initial discharge capacity of the PTCDA is 140 mAh g^{-1} at a current density of 100 mA g^{-1}. With the increasing of current density, the reversible capacities gradually decrease and the Mg-storage capacities of the PTCDA are 105, 60, and 40 mAh g^{-1} at 200, 300, and 500 mA g^{-1}, respectively. The capacity could recover to the initial value when the current density returns to 200 mA g^{-1}. Fig. 2c displays the charge/discharge curves of the PTCDA at a current density of 200 mA g^{-1}. The major discharge plateau is located at 1.7 V and the charge plateau is at 2.1 V. The PTCDA exits a higher working voltage plateau and a small polarization compared with other cathode materials reported in MBs (Fig. 2d). There also exists another minor discharge/charge plateau. Besides, the long-term cycling stability of the PTCDA cathode shown in Fig. 2e presents an initial capacity of 126 mAh g^{-1}, and the reversible capacity retains 100 mAh g^{-1} (at 200 mA g^{-1}) even after 150 cycles. And the Columbic efficiency retains 98% during the long-term cycling. Our results demonstrate that the organic materials enable themselves to act as promising cathodes for high-performance and environmental rechargeable multi-valent ion batteries.

Fig. 3a shows the cyclic voltammetry (CV) curves of the PTCDA at different scanning rates from 0.05 to 0.3 mV s^{-1} in the potential range of 0.6–2.5 V. Two pairs of redox peaks are consistent with the galvanostatic charge/discharge profiles. With the increasing of scanning rate, the peak current value increases and the position of the peaks has a little change, revealing a highly reversible reaction mechanism of the PTCDA. Fig. 3b presents the plots of log (*i*) vs. log (*v*) for the two redox peaks, and the b value represents the slope of the fitted line. The ionic diffusion mainly controls the electrochemical reaction when b = 0.5, and when b = 1, the process is capacitance-dominated contribution [32,33]. The calculated b-values for peak 1 and 2 are 0.99 and 0.98, respectively, indicating a substantial capacity of capacitance contribution. Also, we can calculate the Mg^{2+} diffusion coefficient in organic lattices through the galvanostatic intermittent titration technique (GITT) test. As shown in Fig. 3c, the PTCDA delivers a discharge capacity of 130 mAh g^{-1}, corresponding to about 2 electron transfer during the redox process. The Mg^{2+} diffusivity can be obtained by a constant current pulse via the following formula [34]:

$$D_{GITT} = \frac{4}{\pi\tau}\left(\frac{m_B V_M}{M_B S}\right)^2\left(\frac{\Delta E_s}{\Delta E_\tau}\right)^2 \quad (1)$$

where τ is the constant current pulse time, the molar volume, the mass, and the molar mass of the active materials are replaced by V_M, m_B, and M_B, respectively. ΔE_s and ΔE_τ are two important parameters, the calculation method of which is shown in Fig. S8. S is the contact area between the electrolyte and electrode. Fig. 3d shows the average Mg diffusivity of the PTCDA cathode during the discharge process is about 2×10^{-12} cm^2 s^{-1}, indicating that the $D_{Mg^{2+}}$ of the PTCDA in this battery system is on the same order of magnitude as Mo_6S_8 [35].

To investigate the redox active sites of the functional group and insertion/extraction mechanisms of the PTCDA as Mg-storage material [36], *ex-situ* XRD and *ex-situ* FTIR spectroscopy were performed at different charge/discharge states. The galvanostatic charge/discharge profiles of PTCDA are shown in Fig. 4a. And Fig. 4b shows the corresponding *ex-situ* XRD patterns of the PTCDA. The peaks located at 18° are ascribed to binder polytetrafluoroethylene (PTFE). Upon the discharge process (from point I to IV), the peaks at 24° and 27° corresponding to the (042) and (102) planes gradually disappears. While during the following charge process (from V to VIII), the intensity of these peaks gradually recovers to the initial state again, suggesting that the magnesiation/demagnesiation process involves a reversible structure changes of the PTCDA electrode. To investage the function groups transform mechanism during the cycling, *ex-situ* FTIR analysis was conducted at the selected positions for charge/discharge process (Fig. 4c). During the discharge stage, the peak located at 1700 cm^{-1} diminishes, while a new peak located at 1350 cm^{-1} strengthens, indicating the carbonyl groups (C═O) convert to the enolate groups

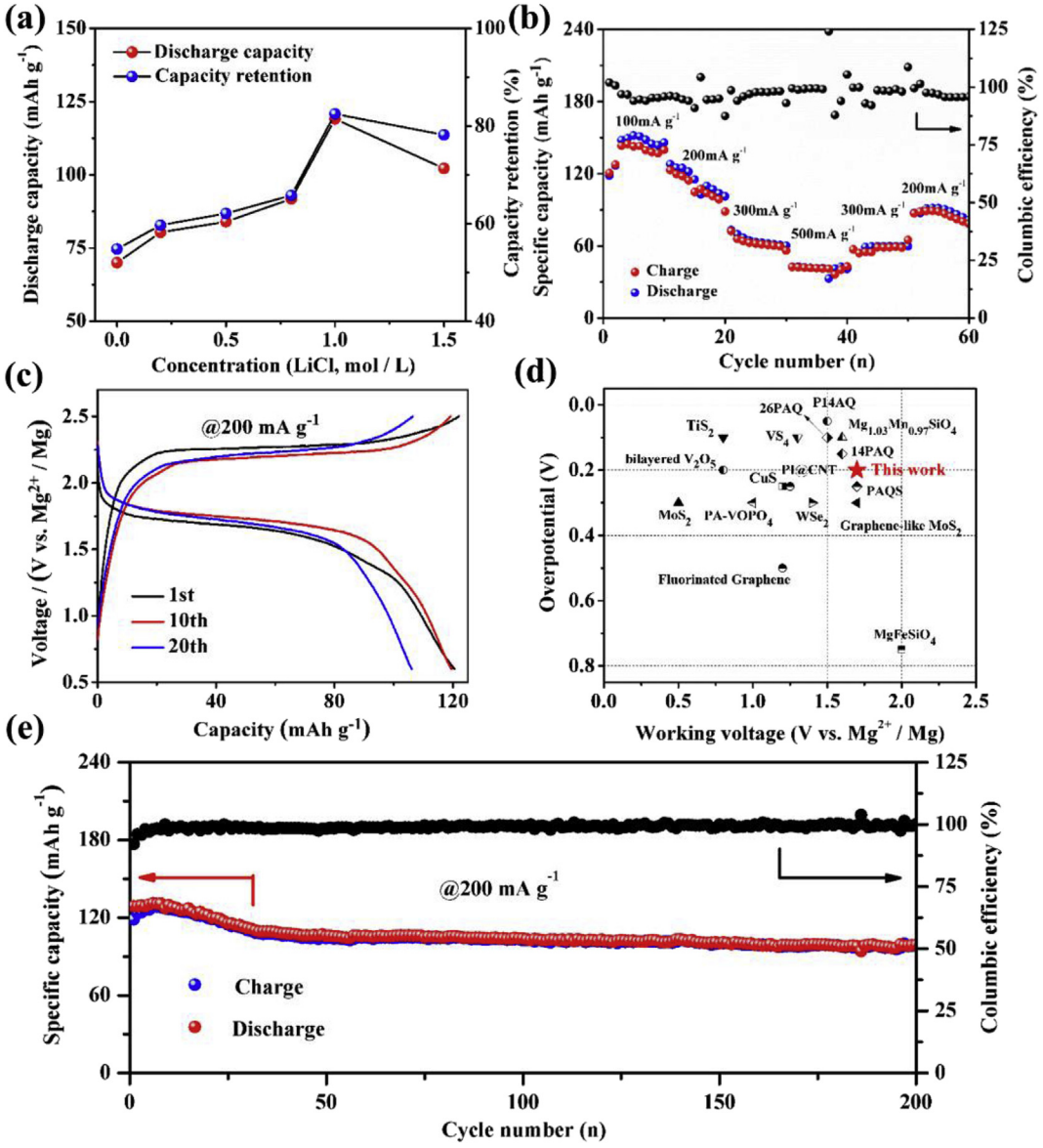

Fig. 2. Electrochemical performance of the PTCDA electrode. (a) Discharge capacity and capacity retention (50th cycle for 0 M and 0.2 M LiCl, 100th cycle for another electrolytes) of the APC electrolytes with different concentrations of LiCl. (b) Rate performance of the PTCDA electrode at current densities of 100, 200, 300, 500 mA g^{-1}, respectively. (c) Galvanostatic charge-discharge curves of PTCDA at a current density of 200 mA g^{-1}. (d) Comparison of the polarization and working voltage of the PTCDA with other Mg-storage materials. (e) The long-term cycling stability of the PTCDA cathode at a current density of 200 mA g^{-1}.

(C–O). During the following charge process, the peak intensity of carbonyl groups gradually recover and the enolate groups gradually diminish. These results represent that the magnesiation/demagnesiation of PTCDA not only involves a reversible structure change but also a transformation mechanism between carbonyl groups and enolate groups [27]. The energy disperse spectroscopy (EDS) elemental mapping of the PTCDA electrode at different charge/discharge states shows the distribution of C, O, Mg, and Cl elements, confirming the reversible magnesiation/demagnesiation behavior of the PTCDA (Fig. 4d and e). The signals of Cl element on fully charged/discharged electrodes likely come from the adsorbed electrolyte on the electrode surface. This result reveals Cl element actually does not involve in the electrochemical reaction. According to the molecule structure diagram of the PTCDA, the center of benzene rings shows a strong positive electricity trend because the four carbonyls of the molecule are electron-withdrawing groups. When $MgCl^+$ is close to the PTCDA molecule, the benzene rings bind easily and take away the chlorine ion due to the positive electricity. According to the DFT theoretical calculation, we come to the conclusion that the molecule structure makes the energy for breaking the Mg–Cl bond less than 3 eV (Fig. S9). This result is also confirmed through X-ray photoelectron spectroscopy (XPS) measurement (Fig. S10). Even in pure APC electrolyte, it has been proved that the Mg^{2+} serves as the intercalation ions instead of $MgCl^+$ (Table S1). Besides, the XPS of Mg (Fig. S11a) and Li element (Fig. S11b) for PTCDA electrodes at different states are detected, revealing the phenomenon that the charge storage is dominated by Mg^{2+} storage instead of Li^+. The atomic ratio between Li and Mg is characterized by inductively coupled plasma optical emission spectrometry (ICP-OES). As charged to 2.5 V, the atomic ratio of Mg:Li was 4.23:1. As discharge proceeds, the atomic ratio of Mg:Li becomes 109.4:1. This result also verifies the charge storage is dominated by Mg^{2+} storage instead of Li^+ (Table S2).

Inspired by the improvement of electrochemical performance of the PTCDA electrode in APC electrolyte with LiCl salt, we investigate the universality of dissolution inhibition in APC electrolyte through adding other salts. We test galvanostatic charge/discharge performances of PTCDA in APC electrolyte with another two salts (NaCl and KCl).

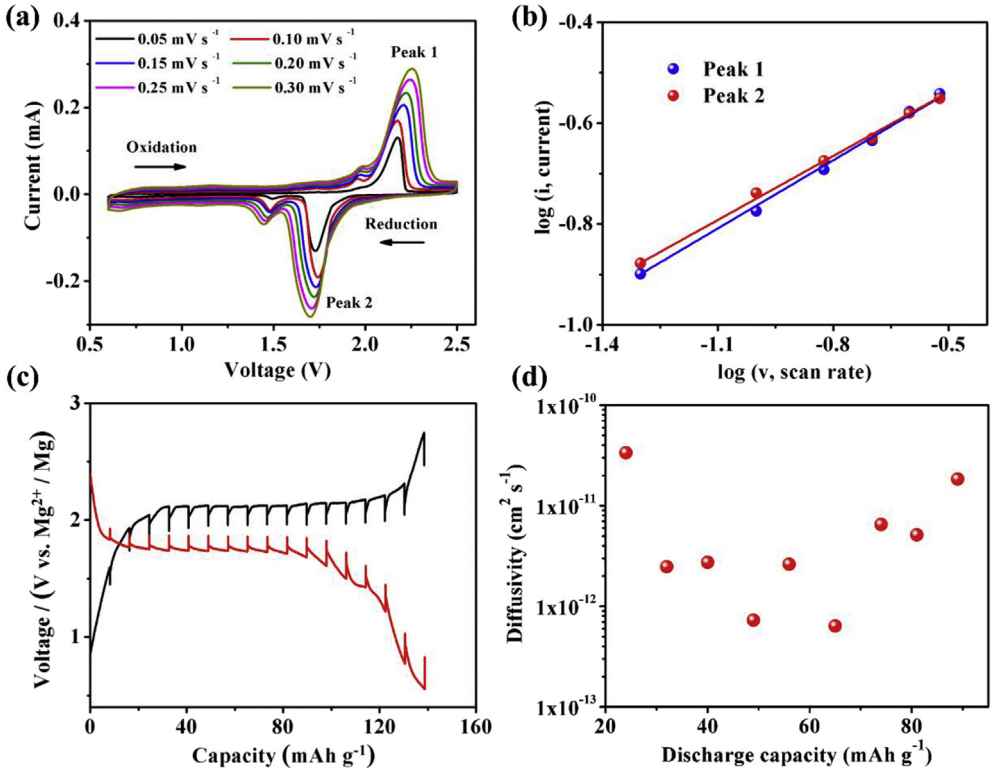

Fig. 3. Kinetic investigation. (a) CV curves of the PTCDA electrode scanned at various rates from 0.05 to 0.3 mV s^{-1} in the potential range of 0.6–2.5 V and (b) corresponding log i *vs.* log v plots at different redox states. (c) GITT curves and (d) the diffusion coefficient of Mg^{2+} calculated based on GITT curves.

Fig. 5a and b shows charge and discharge profiles of PTCDA at the 10th, 20th and 30th cycle in Na-APC and K-APC electrolyte, and the discharge/charge plateaus of the two electrolyte systems remain at 2.1 V/1.7 V, which shows a small changes of the plateau. Fig. 5c shows the cycling stability of PTCDA electrode in Na-APC and K-APC electrolytes, delivering a good cycling stability of 104 and 90 mAh g^{-1} after 65 cycles, respectively. Similar to LiCl, electrolyte containing other dissolved salt also shows an obvious dissolution inhibition effect compared with APC electrolyte and a high discharge plateau.

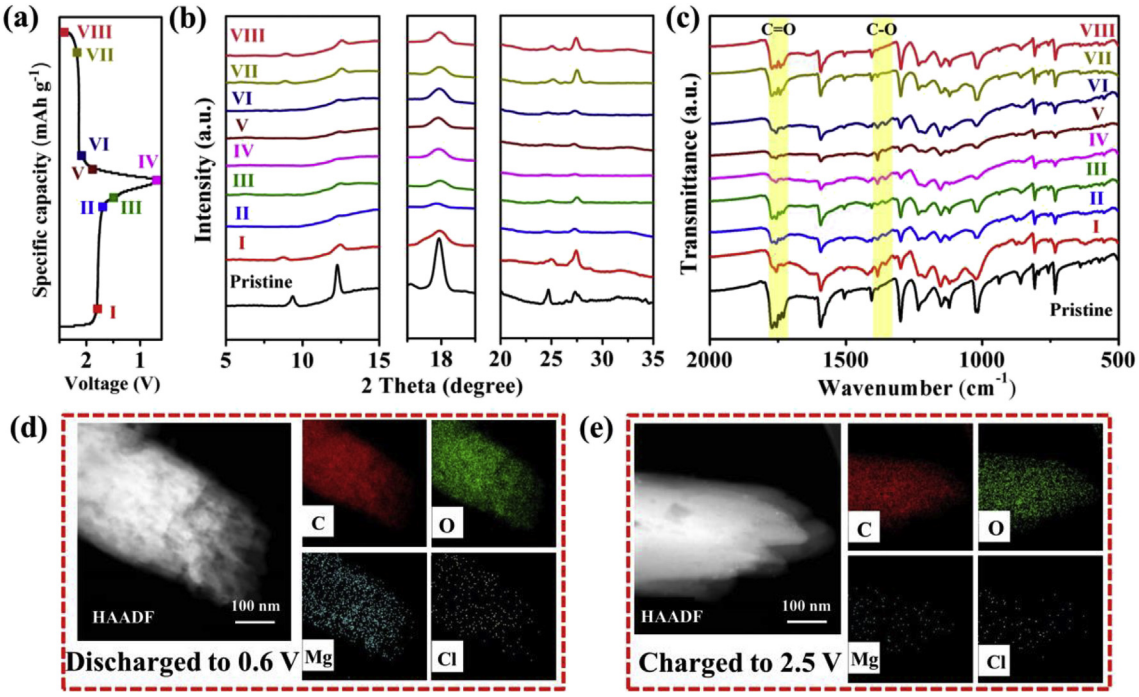

Fig. 4. Structural changes of the PTCDA during charge/discharge process. (a) Galvanostatic charge/discharge profiles of the PTCDA collected at 5th cycle. (b) *Ex-situ* XRD and (c) FTIR curves of the PTCDA at different stages. HAADF image and EDS elemental mappings of the PTCDA at (d) fully-discharged and (e) fully-charged states.

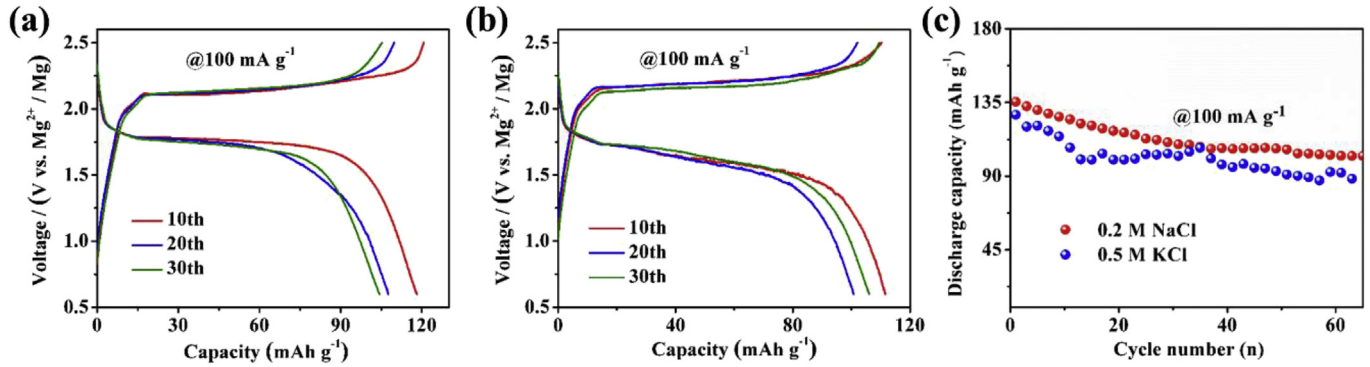

Fig. 5. Electrochemical performance of the PTCDA electrode in APC electrolyte with other salts. Galvanostatic charge-discharge curves at a current density of 100 mA g^{-1} of the PTCDA in APC electrolyte with dissoluble (a) Na- and (b) K- salt. (c) The long-term cycling performance of the PTCDA cathode at a current density of 100 mA g^{-1}.

3. Conclusion

In summary, we have demonstrated that the PTCDA can be served as a cathode material in non-aqueous MBs. Through a salt dissolution inhibition approach for the APC electrolyte with LiCl, the PTCDA exhibits a high Mg-storage capacity, excellent rate capability, and good cycling stability. The evolution mechanism of the PTCDA is revealed by *ex-situ* XRD and FTIR, which shows a good structural reversibility in the potential range from 0.6 to 2.5 V. Furthermore, based on the Mg^{2+}, the electrochemical mechanism of the PTCDA is proved to be the transformation between carbonyl groups (C═O) and enolate groups (C–O). In addition, the dissolution inhibition behavior has also been extended to other soluble salt (NaCl and KCl), achieving remarkable electrochemical performance improvement for the PTCDA. This general approach effectively realizes the maximization of host materials in non-aqueous system, and provides a novel perspective for the high-voltage and high-capacity organic electrode materials applied in the multi-valent ion batteries system with high energy density.

4. Experimental section

4.1. Preparation of all phenyl complex (APC) electrolyte

The all phenyl complex (APC) electrolyte was prepared in two steps according to previous literature [37]. Firstly, we diluted 10 mL aluminum chloride THF complex (Aldrich, 0.5 M in THF) into 5 mL tetrahydrofuran (THF, anhydrous, 99.9%, and removed water by molecular sieves), and under stirring in argon-filled glove box (< 1 ppm of oxygen and water) for at least 6 h. Then the solution was slowly added into 5 mL phenylmagnesium chloride solution (Macklin, 2.0 M in THF) under continuous stirring, and the solution was stirred for another 12 h to form APC electrolyte. The concentration of as-prepared APC electrolyte is 0.25 M.

4.2. Preparation of APC electrolyte with LiCl

This electrolyte was prepared by a simple one-step method. The LiCl (Aladdin, anhydrous, 99.99% metals basis) powder was added into APC electrolyte, and stirring until the LiCl dissolved in APC. The final solution was stirred overnight prior to use. The concentration of hybrid electrolyte was changed with the addition of various amount of LiCl.

4.3. Material characterization

The structure of the samples was characterized by powder X-ray diffraction (XRD) patterns collected on a Bruker AXS D8 Advance powder X-ray diffractometer with Cu K_α irradiation (λ = 1.5406 Å). The morphology of the samples was taken using a field emission scanning electron microscopy (FESEM, JEOL, JSM-7100F). The HAADF and elemental mapping images were taken using a transmission electron microscope (TEM, Tecnai G2 F20). The spectrograms of the samples were collected by ultraviolet–visible spectrophotometer (UV–vis, Lambda 750 S) and Fourier transform infrared spectrometer (FTIR, Nexus). The Li elemental was analyzed by X-ray photoelectron spectroscopy on an ESCALAB 250 Xi spectrometer (XPS, VG Scientific Co., UK).

4.4. Electrochemical characterization

The PTCDA electrodes consist of 80 wt% 3,4,9,10-perylenetetracarboxylic dianhydride (PTCDA), 10 wt% acetylene black and 10 wt % polytetrafluoroethylene (PTFE). The galvanostatic discharge/charge tests were carried out on Land CT2001A battery test system within the voltage range of 0.6–2.5 V (vs. Mg^{2+}/Mg). The cyclic voltammetry (CV) tests were carried out on EC-Lab test system at a scanning rate of 0.05, 0.10, 0.15, 0.20, 0.25, and 0.30 mV s^{-1} respectively. The galvanostatic intermittent titration technique (GITT) tests were carried out on Land CT2001A battery test system with a galvanostatic charge/discharge time of 600 s and followed by a relaxation time for 1800 s.

4.5. DFT calculations

The present calculations were carried out by using the projector augmented wave (PAW) [38] method within DFT, as implemented in the Vienna ab initio simulation package (VASP) [39,40]. The generalized gradient approximation (GGA) in the form of the Perdew-Burke-Ernzerhof (PBE) [41] was used to treat the exchange-correlation energy. A kinetic energy cutoff of 500 eV was used for wave functions expanded in the plane wave basis. All atoms were allowed to relax until the forces were less than 0.05 eV $Å^{-1}$. For the Brillouin-zone sampling, 2 × 2 × 2 k-points were adopted to ensure convergence of the total energy. Ultrasoft pseudopotentials were used to describe the interactions of the ionic core and valence electrons. Referring the energy of state I as the ground one, the activation energy was calculated.

Acknowledgements

This work was supported by the National Key Research and Development Program of China (2016YFA0202603), the National Natural Science Foundation of China (51602239), the Hubei Provincial Natural Science Foundation of China (2016CFB267), and the Fundamental Research Funds for the Central Universities (WUT: 2017III005). K. Zhang would like to thank the Korea Research Fellowship Program of the NRF, funded by the Ministry of Science and ICT (2016H1D3A1906790). We acknowledge Yalong Jiang for the DFT theoretical calculation.

Appendix A. Supplementary data

Supplementary data to this article can be found online at https://doi.org/10.1016/j.nanoen.2019.103902.

References

[1] H. Tian, T. Gao, X. Li, X. Wang, C. Luo, X. Fan, C. Yang, L. Suo, Z. Ma, W. Han, C. Wang, Nat. Commun. 8 (2017) 14083.
[2] W. Kaveevivitchai, A.J. Jacobson, Chem. Mater. 28 (2016) 4593–4601.
[3] D. Aurbach, Z. Lu, A. Schechter, Y. Gofer, H. Gizbar, R. Turgeman, Y. Cohen, M. Moshkovich, E. Levi, Nature 407 (2000) 724–727.
[4] Y. Wang, Z. Liu, C. Wang, X. Yi, R. Chen, L. Ma, Y. Hu, G. Zhu, T. Chen, Z. Tie, J. Ma, J. Liu, Z. Jin, Adv. Mater. 30 (2018) 1802563.
[5] X. Sun, P. Bonnick, L.F. Nazar, ACS Energy Letters 1 (2016) 297–301.
[6] Z. Tao, L. Xu, X. Gou, J. Chen, H. Yuan, Chem. Commun. 18 (2004) 2080–2081.
[7] Y. Liang, R. Feng, S. Yang, H. Ma, J. Liang, J. Chen, Adv. Mater. 23 (2011) 640–643.
[8] Y. Liang, H.D. Yoo, Y. Li, J. Shuai, H.A. Calderon, F.C. Robles Hernandez, L.C. Grabow, Y. Yao, Nano Lett. 15 (2015) 2194–2202.
[9] F. Xiong, Y. Fan, S. Tan, L. Zhou, Y. Xu, C. Pei, Q. An, L. Mai, Nano Energy 47 (2018) 210–216.
[10] S. Tepavcevic, Y.Z. Liu, D.H. Zhou, B. Lai, J. Maser, X.B. Zuo, H. Chan, P. Kral, C.S. Johnson, V. Stamenkovic, N.M. Markovic, T. Rajh, ACS Nano 9 (2015) 8194–8205.
[11] Q. An, Y. Li, H. Deog Yoo, S. Chen, Q. Ru, L. Mai, Y. Yao, Nano Energy 18 (2015) 265–272.
[12] L.F. Wan, J.T. Incorvati, K.R. Poeppelmeier, D. Prendergast, Chem. Mater. 28 (2016) 6900–6908.
[13] Y. NuLi, J. Yang, Y. Li, J. Wang, Chem. Commun. 46 (2010) 3794–3796.
[14] Z. Feng, J. Yang, Y. NuLi, J. Wang, X. Wang, Z. Wang, Electrochem. Commun. 10 (2008) 1291–1294.
[15] T. Mori, T. Masese, Y. Orikasa, Z.D. Huang, T. Okado, J. Kim, Y. Uchimoto, Phys. Chem. Chem. Phys. 18 (2016) 13524–13529.
[16] Y. Orikasa, T. Masese, Y. Koyama, T. Mori, M. Hattori, K. Yamamoto, T. Okado, Z.D. Huang, T. Minato, C. Tassel, J. Kim, Y. Kobayashi, T. Abe, H. Kageyama, Y. Uchimoto, Sci. Rep. 4 (2014) 5622.
[17] P. Sharma, D. Damien, K. Nagarajan, M.M. Shaijumon, M. Hariharan, J. Phys. Chem. Lett. 4 (2013) 3192–3197.
[18] H. Wu, K. Wang, Y. Meng, K. Lu, Z. Wei, J. Mater. Chem. 1 (2013) 6366–6372.
[19] X. Han, C. Chang, L. Yuan, T. Sun, J. Sun, Adv. Mater. 19 (2007) 1616–1621.
[20] W. Luo, M. Allen, V. Raju, X.L. Ji, Adv. Energy Mater. 4 (2014) 1400554.
[21] H. Wang, S. Yuan, D. Ma, X. Huang, F. Meng, X. Zhang, Adv. Energy Mater. 4 (2014) 1301651.
[22] H. Dong, Y.L. Liang, O. Tutusaus, R. Mohtadi, Y. Zhang, F. Hao, Y. Yao, Joule 3 (2019) 782–793.
[23] B.F. Pan, J.H. Huang, Z.X. Feng, L. Zeng, M.N. He, L. Zhang, J.T. Vaughey, M.J. Bedzyk, P. Fenter, Z.C. Zhang, A.K. Burrell, C. Liao, Adv. Energy Mater. 6 (2016) 1600140.
[24] X.L. Fan, F. Wang, X.X. Ji, R.X. Wang, T. Gao, S.Y. Hou, J. Chen, T. Deng, X.G. Li, L. Chen, C. Luo, L.N. Wang, C.S. Wang, Angew. Chem. Int. Ed. 57 (2018) 7146–7150.
[25] J. Bitenc, K. Pirnat, T. Bancic, M. Gaberscek, B. Genorio, A. Randon-Vitanova, R. Dominko, Chemsuschem 8 (2015) 4128–4132.
[26] B. Pan, D. Zhou, J. Huang, L. Zhang, A.K. Burrell, J.T. Vaughey, Z. Zhang, C. Liao, J. Electrochem. Soc. 163 (2016) A580–A583.
[27] I.A. Rodriguez-Perez, Y. Yuan, C. Bommier, X. Wang, L. Ma, D.P. Leonard, M.M. Lerner, R.G. Carter, T. Wu, P.A. Greaney, J. Lu, X. Ji, J. Am. Chem. Soc. 139 (2017) 13031–13037.
[28] I. Shterenberg, M. Salama, Y. Gofer, E. Levi, D. Aurbach, MRS Bull. 39 (2014) 453–460.
[29] H.D. Yoo, I. Shterenberg, Y. Gofer, G. Gershinsky, N. Pour, D. Aurbach, Energy Environ. Sci. 6 (2013) 2265–2279.
[30] L. Fan, R. Ma, J. Wang, H. Yang, B. Lu, Adv. Mater. 30 (2018) 1805486.
[31] L. Suo, Y. Hu, H. Li, M. Armand, L. Chen, Nat. Commun. 4 (2013) 1481.
[32] L. Zhou, K. Zhang, J. Sheng, Q. An, Z. Tao, Y.-M. Kang, J. Chen, L. Mai, Nano Energy 35 (2017) 281–289.
[33] T. Brezesinski, J. Wang, S.H. Tolbert, B. Dunn, Nat. Mater. 9 (2010) 146–151.
[34] E. Deiss, Electrochim. Acta 50 (2005) 2927–2932.
[35] M.D. Levi, E. Lancry, H. Gizbar, Y. Gofer, E. Levi, D. Aurbach, Electrochim. Acta 49 (2004) 3201–3209.
[36] B. Pan, Z. Feng, N. Sa, S.D. Han, Q. Ma, P. Fenter, J.T. Vaughey, Z. Zhang, C. Liao, Chem. Commun. 52 (2016) 9961–9964.
[37] N. Pour, Y. Gofer, D.T. Major, D. Aurbach, J. Am. Chem. Soc. 133 (2011) 6270–6278.
[38] G. Kresse, D. Joubert, Phys. Rev. B 59 (1999) 1758.
[39] G. Kresse, J. Furthmüller, Phys. Rev. B 54 (1996) 11169.
[40] G. Kresse, J. Furthmüller, Comput. Mater. Sci. 6 (1996) 15–50.
[41] J. Perdew, K. Burke, M. Ernzerhof, Phys. Rev. Lett. 77 (1996) 3865.

Lianmeng Cui received his B.S. degree in Material Science and Engineering from Shandong University of Science and Technology in 2017. He is currently working toward the M.S. degree in Materials Science and Engineering from Wuhan University of Technology. His current research focuses on synthesis and characterization of advanced materials for emerging energy storage devices.

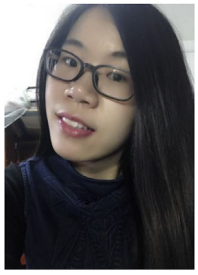

Limin Zhou received her M.S. degree from College of Chemistry at Nankai University in 2015. She is currently working toward the Ph.D. degree and her current research focuses on synthesis and characterization of advanced materials for emerging energy storage devices.

Kai Zhang received his Ph.D. in 2015 and B.S. in 2010 from College of Chemistry at Nankai University (China) under the supervision of Professor Jun Chen. Currently, he is a postdoctoral researcher in the group of Professor Yong-Mook Kang at the Department of Energy and Materials Engineering in Dongguk University, Seoul, Korea. His research focuses on lithium-ion, lithium-sulfur, and sodium-ion batteries.

Fangyu Xiong received his B.S. degree in Material Physics from Wuhan University of Technology in 2016. He is currently working toward the Ph.D. degree and his current research interest focuses on electrode materials for emerging energy storage devices.

Shuangshuang Tan received his B.S. degree in Material Science and Engineering from Wuhan University of Technology in 2016. He is currently working toward the Ph.D. degree and his current research focuses on the energy storage materials and devices.

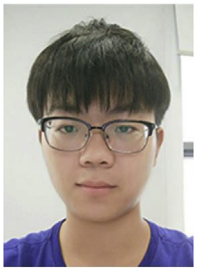

Maosheng Li received his B.S. degree in Material Science and Engineering from Beijing University of Chemical Technology in 2017. He is currently working toward the M.S. degree in Materials Science and Engineering from Wuhan University of Technology. His current research focuses on advanced materials for energy storage devices.

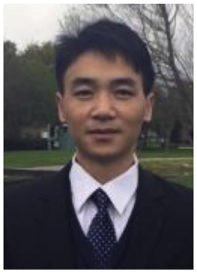

Qinyou An is Associate Professor of Materials Science and Engineering at Wuhan University of Technology (WUT). He received his Ph.D. degree from WUT in 2014. He carried out his postdoctoral research in the laboratory of Prof. Yan Yao at the University of Houston in 2014–2015. Currently, his research interest includes energy storage materials and devices.

Yong-Mook Kang completed B.S. (1999), M.S. (2001), and Ph.D. (2004) at Korea Advanced Institute of Science and Technology. He has been a senior researcher at Samsung SDI Co., LTD. He is currently a professor in Department of Energy and Materials Engineering at Dongguk University-Seoul, as well as a TWAS (World Academy of Sciences for Developing Countries) young affiliate. His research area covers electrode or catalyst materials for Li rechargeable batteries and various post Li batteries, such as Li–O2 battery, Na rechargeable battery, etc. In 2015, he has been appointed as RSC (Royal Society of Chemistry) fellow and representative in Korea.

Liqiang Mai is Changjiang Scholar Chair Professor of Materials Science and Engineering at Wuhan University of Technology (WUT). He is the winner of the National Natural Science Fund for Distinguished Young Scholars and Fellow of the Royal Society of Chemistry. He received his Ph.D. from WUT in 2004 and carried out his postdoctoral research with Prof. Zhong Lin Wang at Georgia Institute of Technology in 2006–2007.He worked as an advanced research scholar with Prof. Charles M. Lieber at Harvard University in 2008–2011 and Prof. Peidong Yang at University of California, Berkeley in 2017. His current research interests focus on new nanomaterials for electrochemical energy storage and micro/nano energy devices.